(article starts on next page)

Influence of Yttrium Doping on the Oxidation of Mo(Si,Al)$_2$ in Air at 1500 °C

Aina Edgren[1,2] · Lars-Gunnar Johansson[3] · Erik Ström[2] ·
Magnus Hörnqvist Colliander[1]

Abstract

Mo(Si,Al)$_2$ with different yttrium (Y) additions (up to 2 at.%) was synthesised by dry powder mixing followed by compaction and sintering. In as-sintered materials, Y was present as yttrium aluminium garnet. The materials were exposed in air at 1500 °C for up to 250 h to study the effect of Y on oxidation behaviour. The oxides formed were investigated using scanning electron microscopy (SEM)-based techniques and X-ray diffraction. While the Y-free Mo(Si,Al)$_2$ formed a scale consisting of Al$_2$O$_3$ and a small amount of mullite, the Y-containing samples formed oxides containing both yttrium silicate and larger fractions of mullite, in addition to Al$_2$O$_3$. Oxidation rate, scale spallation, as well as the evaporation of Mo, all increased with Y addition.

Keywords Mo(Si,Al)$_2$ · Oxidation · Spallation · Reactive elements

Introduction

Replacing fossil fuel-based industrial heating processes with electrical solutions offers an efficient route to reducing the emission of greenhouse gasses. This is particularly important for high temperature processes (above 1000 °C) due to the high energy consumption [1]. Indirect Joule heating, using electric resistance heating elements, is a flexible and mature technology with high efficiency and low cost [2]. It is used in different applications today, mainly at lower temperatures, but also to some extent at higher temperatures. At high temperatures, MoSi$_2$-based elements are often used due

✉ Magnus Hörnqvist Colliander
   magnus.colliander@chalmers.se

1   Department of Physics, Chalmers University of Technology, 41296 Gothenburg, Sweden

2   Kanthal AB, P.O. Box 502, 734 27 Hallstahammar, Sweden

3   Department of Chemistry and Chemical Engineering, Chalmers University of Technology, 41296 Gothenburg, Sweden

to the high melting point and excellent corrosion resistance [3–5]. Above 1000 °C $MoSi_2$ forms a SiO_2 scale which is protective in high pO_2, but less efficient in low pO_2 environments. By partially substituting Si by Al to form $Mo(Si,Al)_2$, this problem can be overcome due to the formation of an Al_2O_3 scale during oxidation. Al_2O_3 not only shows better protective properties in reducing atmospheres, but also better adhesion in high gas flows [6]. Furthermore, the addition of Al also supresses pesting, which is a problem in the case of $MoSi_2$ [7–11]. Therefore, $Mo(Si,Al)_2$ has great potential as heating elements in high-temperature industrial furnaces operating in both reducing and oxidising environments, for example within the steel industry, a sector which gives rise to very high CO_2 emissions [1, 2].

However, the $Mo(Si,Al)_2$ elements used today are designed to operate in the kW power range. To be used in large MW-range industrial furnaces, an upscaling of the heating systems and an associated increase in the dimensions of the heating elements, for example the diameter, is needed. Even though the oxidation properties of $Mo(Si,Al)_2$ at elevated temperature are excellent, it has been reported that large diameter elements may be somewhat more susceptible to oxide scale spallation (based on company (Kanthal AB) internal communications). From an application point of view, it is important to mitigate spallation, as it limits the service life of the elements. Alloying with small amounts of the so-called reactive elements (REs), for example Y, Zr and Hf, is known to greatly improve the oxidation behaviour and reduce scale spallation of Al_2O_3-forming alloys, for example FeCrAl alloys [12–14]. Also, the oxidation properties of SiO_2-forming Mo-Si based materials, such as Mo-Si-B and $MoSi_2$, can be improved by RE doping. Additions of Y have been shown to improve the oxidation behaviour of Mo-Si-B alloys in both the intermediate (650–1000 °C [15–17]) and in the high temperature (1000–1400 °C [15, 18, 19]) range. Y addition (3.3 at.%) to $MoSi_2$ has been reported to improve the oxidation properties at intermediate temperatures [16]. In investigations performed at higher temperatures (up to 1600 °C), Y was added as both as metal (3.3 at.% Y) [20] and as Y_2O_3 (15 vol%) [21]. However, the addition led to rapid oxidation and oxide scale spallation [20, 21]. It was reported that $Y_2Si_2O_7$ was present in the outer part of the SiO_2 scale [20, 21], but the origin of this phase, and its role in the oxidation process, was not discussed.

Based on the above observations, it is interesting to explore the possible effects of REs in Al_2O_3-forming $Mo(Si,Al)_2$, but no such studies have been reported. In this work, the effect of Y additions (up to 2 at.%) on the oxidation rate and scale spallation of $Mo(Si,Al)_2$ for up to 250 h at 1500 °C has been investigated. We show that the presence of Y promotes the formation of mullite in the oxide scale, and that the formation of liquid phase in the scale leads to increased oxidation rates and spallation. The results clearly indicate that Y doping is not suitable for $Mo(Si,Al)_2$-based materials.

Materials and Methods

Four materials with different Y additions (0.1, 0.5, 1.0 and 2.0 at.%), and a Y-free reference material with composition similar to commercial grade $Mo(Si,Al)_2$ heating elements, were synthesized. Powders of elemental Mo, Y (both 99.9% purity,

Table 1 Chemical composition (at.%) of $Mo(Si,Al)_2$ and $Mo_5(Si,Al)_3$				
$Mo(Si,Al)_2$	32.1 Mo	35.3 Si	29.4 Al	3.2 O
$Mo_5(Si,Al)_3$	58.5 Mo	33.5 Si	5.9 Al	2.2 O

Cerac, Inc.), Si (99.99% purity, Wacker) and Al (99.5% purity, GoodFellow) were mixed and reacted to form $Mo(Si,Al)_2$. The reacted product was milled to a powder having a specific surface area < 1.6 m^2/g. The surface area was measured using the Brunauer–Emmett–Teller (BET) method. Al_2O_3 (AKP-30, 99.99% purity, Sumitomo Chemicals) was added as grain refiner. The powders were compacted to rods using cold isostatic pressing (CIP) and sintered in H_2 gas at 1650 °C. The sintered rods were ground with 500 mesh SiC to remove the surface layer prior to cutting. Sample thickness was 5 mm, and the diameter was 10 mm.

Multiple samples of each composition were placed in a box furnace for oxidation exposures in air at 1500 °C (ramp time from room temperature was 5 h). Each sample was placed in an open cylindrical alumina crucible. After 24 h at the target temperature, the furnace was turned off and the samples were air cooled to below 200 °C. The mass of the samples and the spalled oxide (collected in the Al_2O_3 crucibles) were measured. The exposure procedure was repeated, resulting in samples being oxidised for 24, 50, 100 and 250 h.

Cross sections and surfaces of the as-sintered material and materials being oxidised for 24, 50 and 250 h were analysed by back scatter electron (BSE) imaging and energy dispersive X-ray spectroscopy (EDS) in a FEI Quanta 200 FEG ESEM scanning electron microscope (SEM) using an accelerating voltage of 20 kV, and by X-ray diffraction (XRD) in a Bruker D8 Advance system equipped with a Cu-anode.

Results and Discussion

Microstructure of As-Sintered Materials

The as-sintered reference material consisted of three phases, $Mo(Si,Al)_2$, $Mo_5(Si,Al)_3$ and Al_2O_3 (approximately 79 vol%, 7 vol% and 14 vol%, respectively). The chemical composition of the intermetallic regions was measured by EDS and is given in Table 1. The apparent oxygen content in the intermetallics is attributed to the presence of nano-sized Al_2O_3 particles as previously reported [4, 5, 22, 23].

In the Y-containing materials, a fourth phase, YAG (yttrium aluminium garnet, $Y_3Al_5O_{12}$) was found, see Fig. 1. Indeed, elemental mapping using SEM–EDS showed that Y was only detected in the YAG particles. Evidently, Y, which was added in elemental form, has oxidised and formed YAG during fabrication of the composite. This is not unexpected, considering that the oxidation of Y by Al_2O_3 is spontaneous [24]. As anticipated, analysis by XRD showed that the YAG content increased with the amount of Y added (Fig. 1b). The volume fraction of YAG in the different materials (determined by image analysis of SEM–EDS maps) is given in Table 2. The volume fractions of $Mo(Si,Al)_2$, $Mo_5(Si,Al)_3$ and Al_2O_3 were similar to
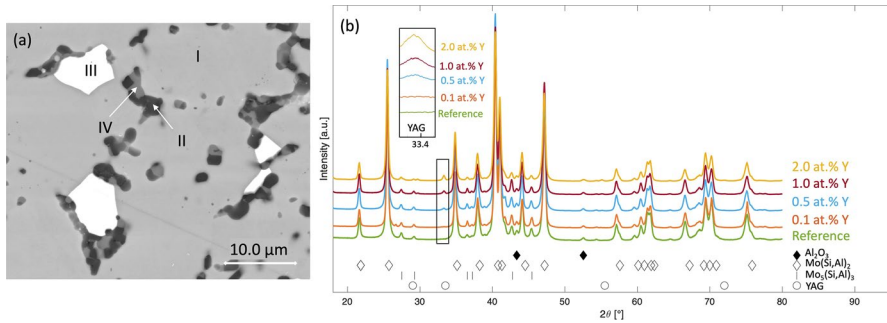
Fig. 1 a BSE image of as-sintered 2 at.% Y material. (I) $Mo(Si,Al)_2$, (II) Al_2O_3, (III) $Mo_5(Si,Al)_3$ and (IV) YAG. **b** XRD diffractogram of the materials in the as-sintered condition

Table 2 Volume fraction of YAG in the Y-alloyed $Mo(Si,Al)_2$ materials

Material	0.1 at.% Y	0.5 at.% Y	1 at.% Y	2 at.% Y
Vol% YAG	0.1	0.5	1.4	2.6

the reference material. The YAG particles tended to be in contact with Al_2O_3 grains, see the BSE image of the 2 at.% Y sample in Fig. 1a. EDS analysis showed that while some YAG particles were very close to stochiometric (15 at.% Y, 25 at.% Al and 60 at.% O), most YAG particles featured traces of Mo and Si. The average composition of the "contaminated" YAG particles was: (at.%) 12 Y, 25 Al, 57 O, 3.0 Si and 3.5 Mo. The association of YAG with Al_2O_3 and the frequent Si-Mo "contamination" of the particles provides clues to the formation of the YAG particles during fabrication. It is suggested that Y initially is present in a mixed Mo-Si-Al phase and that Y is then oxidised by Al_2O_3, forming YAG. The apparent contamination of the YAG particles then corresponds to the remains of the original, Y-containing phase. The formation of YAG through oxidation by Al_2O_3 is further supported by the fact that the YAG particles were frequently found in contact with Al_2O_3 particles.

Mass Gain and Spallation

Gravimetry showed that while the reference material gained mass (with mass gains in accordance to previous studies on oxidation at 1500 °C by Ingemarsson et al. [4]), during oxidation exposure, the materials containing > 0.1% Y exhibited mass losses which increased with the Y content, see Fig. 2a. Ingemarsson reported very limited scale spallation from $Mo(Si,Al)_2$ and it was suggested that the mass loss due to MoO_3 evaporation (which is discussed below) could be neglected [4] (see below). In agreement with [4], very little spalled oxide was collected from the reference material, see Fig. 2b. In contrast, the Y-containing materials suffered significant scale spallation which increased with both Y-content and oxidation time. We suggest that spallation occurred during cooling of the sample, as a "snapping" sound could be heard when the furnace was opened. As mentioned, the samples can also lose mass due to Mo evaporation (as MoO_3). To calculate the loss of Mo by volatilization,
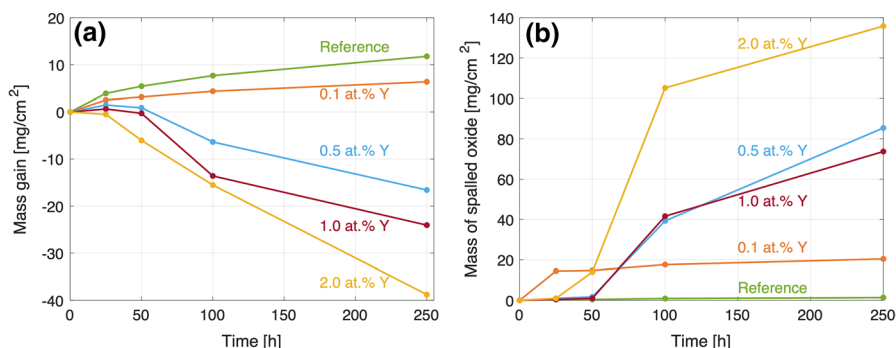
Fig. 2 Mass change plotted against time for Y-doped $Mo(Si,Al)_2$ materials exposed at 1500 °C, **a** mass change of sample only, **b** mass of spalled scale

two different approaches were tried: (1) from the gravimetric data. In this approach, the mass lost by Mo evaporation corresponds to the difference between the original sample mass and the mass arrived at by adding the mass of spalled scale to the mass of the oxidised sample and subtracting the mass of oxygen in the oxide (remaining + spalled) (the cross-section SEM analysis provides information on the thickness and phase composition of the remaining scale, the spalled scale is assumed to have the same composition as the remaining scale). (2) this approach uses the amount of Si(IV) in the oxide (scale and spalled). Thus, the Si(IV) (silica, yttrium disilicate and mullite) in the scale is considered to originate from the oxidation of $Mo_5(Si,Al)_3$[1] which forms a continuous layer at the oxide scale/substrate interface. Thus, Mo oxidation can only occur if Si is also oxidised:

$$Mo_5Si_3 + 211/2\,O_2 \rightarrow 5\,MoO_3 + 3\,SiO_2 \qquad (1)$$
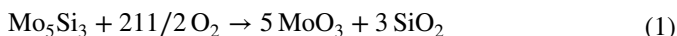
In the case of the Y-containing materials, the amount of Mo loss obtained from gravimetry was much greater than that estimated from the amount of silicon in the scale. The discrepancy is attributed to a failure to collect all spalled oxide. This implies that the gravimetric data in Fig. 2b underestimates the scale spallation of the Y-containing materials.

Oxidation of Y-Free Reference Material

The oxide scale formed on the reference material was relatively dense and mainly consisted of Al_2O_3, see Fig. 3. The measured thickness of the oxide scale (see Figs. 3 and 4a) was in good agreement with the mass gain data. In accordance with [4], a $Mo_5(Si,Al)_3$ layer is sandwiched between the oxide scale and the

---

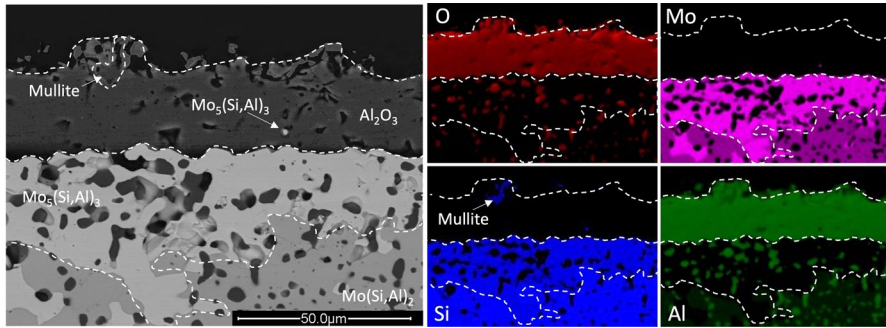[1] $Mo_5(Si,Al)_3$ is replaced by Mo_5Si_3 in (1) to simplify.

Fig. 3 The reference material after 24 h oxidation. The BSE image shows the Al_2O_3 scale with a mullite region, the $Mo_5(Si,Al)_3$ layer and the bulk material which is dominated by $Mo(Si,Al)_2$. EDS maps show the distribution of O, Mo, Si (with mullite indicated) and Al. A detached $Mo_5(Si,Al)_3$ particle in the Al_2O_3 scale is indicated by an arrow

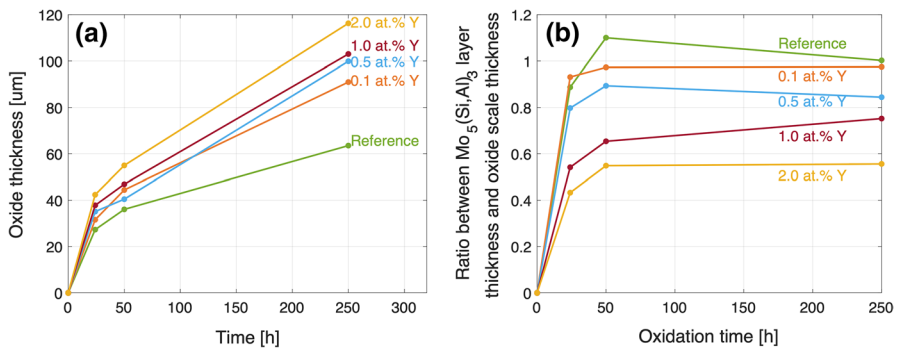**Fig. 4** **a** Thickness of the oxide scale; **b** ratio between Mo5(Si,Al)3 layer thickness and oxide scale thickness. The oxide and $Mo_5(Si,Al)_3$ layer thickness was calculated using at least 20 measurements per point

$Mo(Si,Al)_2$-dominated bulk material. This is a result of the preferential oxidation of Al, which causes $Mo(Si,Al)_2$ to transform to $Mo_5(Si,Al)_3$ [3–5]:

$$(25x + 10)\,MoSiAl + 105x/4\,O_2 \rightarrow 35x/2\,Al_2O_3 + 10\,MoSi_{1+x}Al_{1-x} + 5x\,Mo_5Si_3 \tag{2}$$
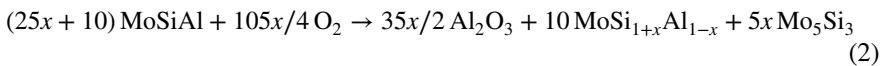
The $Mo_5(Si,Al)_3$ layer was significantly lower in Al (ca 3 at.%) compared to the $Mo_5(Si,Al)_3$ grains in the bulk material (ca 5.9 at.%). However, there was no detectable aluminium gradient in the layer itself. It contained a high fraction of voids, which are attributed to the volume decrease associated with the phase transformation from $Mo(Si,Al)_2$ to $Mo_5(Si,Al)_3$. The many Al_2O_3 particles occurring in the $Mo_5(Si,Al)_3$ layer are considered to correspond to Al_2O_3 particles present in the bulk material (see Fig. 1), which have become incorporated in the $Mo_5(Si,Al)_3$ layer as it grows inward. The $Mo_5(Si,Al)_3$ layer and the oxide scale were similar in thickness, see Figs. 3 and 4b, in accordance with previous research [4].
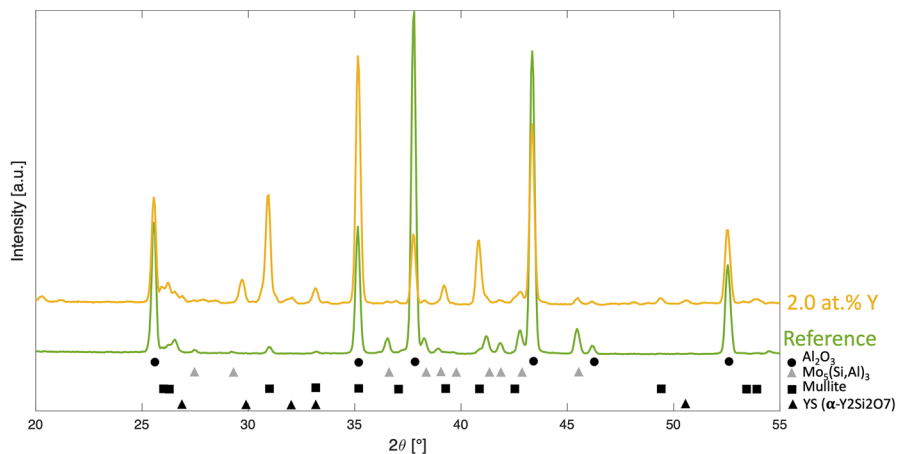
Fig. 5 XRD diffractograms of the reference material and the 2 at.% Y material after 50 h exposure

As a consequence of reaction (2), and in accordance with Ingemarsson et al. [3, 4], an Al-gradient was present in the $Mo(Si,Al)_2$ underneath the $Mo_5(Si,Al)_3$ layer. In the present study, the Al content decreased from 29.4 at.% in the bulk to 24.3 at.% at the $Mo_5(Si,Al)_3$ layer/$Mo(Si,Al)_2$ interface. Due to the stoichiometry of $Mo(Si,Al)_2$, there is a corresponding Si gradient with opposite sign.

Si-rich pockets were observed in the outer part of the Al_2O_3 scale, which were identified as mullite ($3Al_2O_3 \cdot 2SiO_2$) based on SEM–EDS and XRD analysis, see Figs. 3 and 5. The volume fraction of mullite in the Al_2O_3 scale was just a few percent. The formation of mullite during $Mo(Si,Al)_2$ oxidation has been reported previously [4, 25, 26], and was suggested to originate from the oxidation of $Mo_5(Si,Al)_3$ particles which have become incorporated into the Al_2O_3 scale [4] (reaction 1). A particle of this kind is indicated in Fig. 3. These particles are expected to oxidise sequentially, Al first, then Si and lastly Mo, as a result of the different oxygen affinity of the elements (reaction 1).

As mentioned, mullite was only found in the outer part of the oxide scale. The absence of mullite in the inner part of the scale is attributed to the low oxygen activity caused by the oxidation of Al at the $Mo_5(Si,Al)_3$/Al_2O_3 interface, which renders Si(IV) (SiO_2, yttrium disilicate and mullite) thermodynamically unstable. Indeed, in this part of the scale, Si was only detected in the unoxidised $Mo_5(Si,Al)_3$ particles. As the Al_2O_3/$Mo_5(Si,Al)_3$ interface moves inward due to oxidation, the distance between the detached particles and the $Mo_5(Si,Al)_3$ layer increases, diminishing the effect of the strongly reducing interface. When the oxygen activity becomes high enough, oxidation of Si in the particles to the IV-valent state becomes spontaneous (reaction 1).

Ingemarsson et al. [4] report that the SiO_2 generated in this way formed a melt with traces of Na_2O (Na originated from the material synthesis), the melt penetrating the scale via the Al_2O_3 grain boundaries. It was argued that the MoO_3 formed (reaction 1), dissolved in the melt and then evaporated at the oxide scale surface [4].
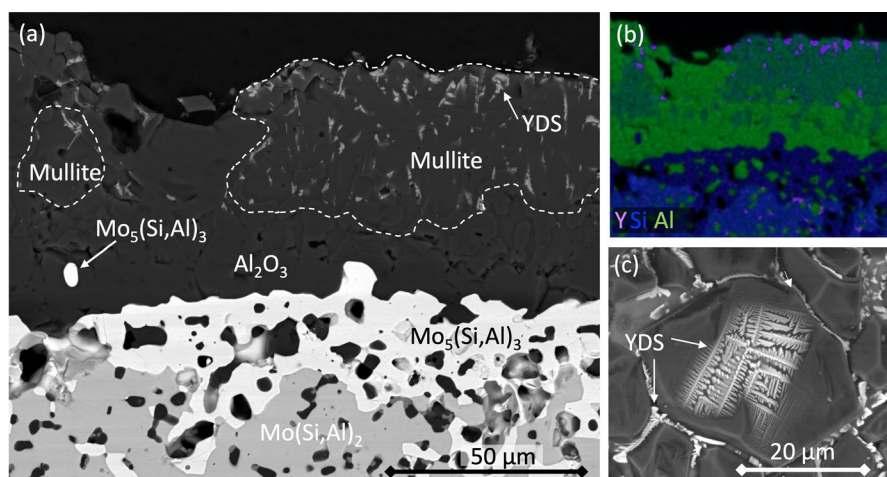
Fig. 6 2 at.% Y after 50 h exposure, **a** cross-section BSE image with the different phases indicated, **b** EDS map showing Y, Si and Al, **c** BSE image of surface Al_2O_3 grain with dendritic YDS

Also, the silicate melt was reported to react with Al_2O_3, forming mullite [4]. It is noted that Na is absent in the present study because the method used for fabrication of the ceramic composite does not involve Na-containing reactants.

Effect of Y on Oxidation

Formation of Mullite and Yttrium Disilicate in the Oxide Scale

In comparison with the reference material, the Y-containing materials formed thicker oxide scales with higher mullite content, see Figs. 4, 6 and 7. The 2 at.% Y material exhibited mullite regions with sizes up to about 100 μm (Fig. 6), while the mullite regions only reached a few tens of μm in the other materials. In addition, the oxide scale also contained a Y- and Si-rich oxide which was identified as yttrium disilicate (YDS, monoclinic α-$Y_2Si_2O_7$) by XRD (Fig. 5) and EDS. This phase has previously been observed to form in the SiO_2 scale of Y-alloyed $MoSi_2$ [20, 21]. The dendritic morphology of the YDS grains, see Figs. 6 and 7, indicates that YDS has crystallised from a melt. After all exposure times and for all materials, the Si(IV)-containing oxides mullite and YDS, were only present in the outer part of the oxide scale, while the inner part of the scale was dominated by Al_2O_3, together with a few detached $Mo_5(Si,Al)_3$ particles, which remained unoxidised due to low oxygen activity, see Fig. 6. Similar to the reference material, these particles will oxidise as the Al_2O_3/$Mo_5(Si,Al)_3$ interface moves inward.

Preferential Oxidation of Aluminium is Affected by Y-Alloying

In accordance with [4], the source of Si(IV) in the scale on the reference material is considered to be the detached $Mo_5(Si,Al)_3$ particles (see Fig. 3). It is tempting
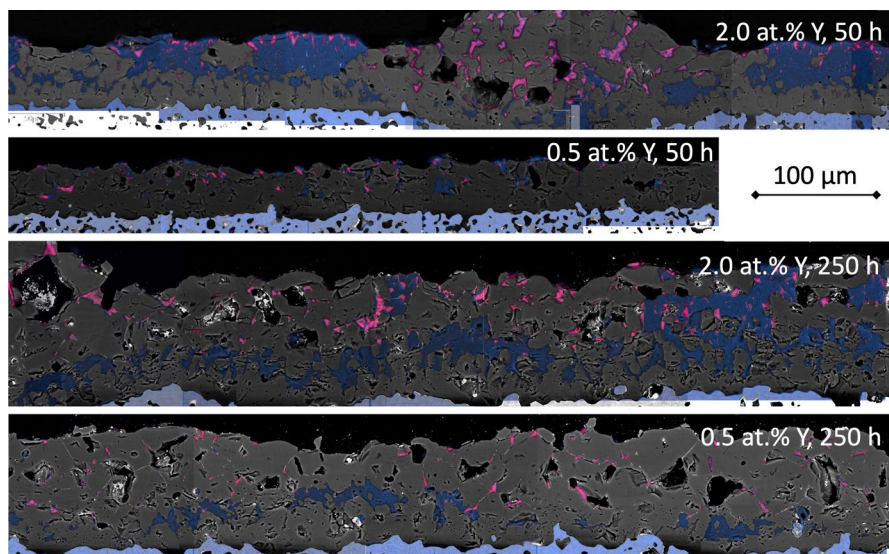
Fig. 7 Cross sections from materials with 2 and 0.5 at.% Y oxidised for 50 and 250 h. Pink regions indicate YDS and blue regions in the oxide scale indicate mullite. Al_2O_3 is shown in grey. $Mo_5(Si,Al)_3$ underneath the scale is blue/white. The scale bar applies for all images. A magnification showing the dendritic structure of YDS is shown in the lower right corner of the figure

to assume that this is also the case for the Y-containing materials, especially since the ratio between the thickness of the $Mo_5(Si,Al)_3$ layer and the oxide scale thickness decreases with increased Y content. For example, after 250 h of oxidation, the thickness of the $Mo_5(Si,Al)_3$ layer was only around 50% of the oxide scale thickness in case of the 2 at.% Y material, while the ratio was close to unity in the case of the reference material, see Fig. 4. Furthermore, taking into account that the Y alloyed materials had much higher spallation than the reference material, the "true" ratio between $Mo_5(Si,Al)_3$ layer and the oxide (remaining and spalled) is much lower than indicated in Fig. 4. However, in order to account for the much greater amount of Si(IV) in the oxides on the Y-containing materials (compare Figs. 3 and 6), this would require a correspondingly higher number density, or larger size, of detached $Mo_5(Si,Al)_3$ particles. No such increase was observed in the SEM/EDS analysis, indicating that the greater amount of Si(IV) in the scale is due to that the preferential oxidation of Al to form a protective Al_2O_3 scale, which is typical for the reference material, works less well in the presence of Y. Also, because the formation of the $Mo_5(Si,Al)_3$ layer is a direct consequence of the preferential oxidation of Al (reaction 2), the formation of relatively thin $Mo_5(Si,Al)_3$ layers on Y-containing materials can also be attributed to the oxidation process being less selective for Al.

Transport of Y from YAG in Bulk to YDS in Oxide Scale

It was noted that the YAG content in the $Mo_5(Si,Al)_3$ layer was very low regardless of oxidation time. After 250 h oxidation of the 2 at.% Y material, the YAG

content in the $Mo_5(Si,Al)_3$ layer was < 0.3 vol%, compared to about 2.6 vol% in the $Mo(Si,Al)_2$-dominated interior of the material. This implies that the YAG particles in the bulk material dissolve as they become incorporated in the inward-growing $Mo_5(Si,Al)_3$ layer.

The loss of YAG in the $Mo_5(Si,Al)_3$ layer corresponds to the appearance of $Y_2Si_2O_7$ in the outer part of the oxide scale. It is argued that the transport of Y, from the dissolving YAG particles in the $Mo_5(Si,Al)_3$ layer to the outer part of the Al_2O_3 scale, is a by-product of the growth of the Al_2O_3 scale. Thus, it is argued that Al_2O_3 scale growth occurs by cathodic reduction in O_2 at the top of the Al_2O_3 layer and anodic oxidation of Al at the $Al_2O_3/Mo_5(Si,Al)_3$ layer interface. Under the influence of this potential difference, Y^{3+} ions migrate towards the scale surface via the Al_2O_3 grain boundaries. In the outer part of the scale, where Si(IV) is present, Y^{3+} reacts to form a melt together with SiO_2 and Al_2O_3. Upon cooling, $Y_2Si_2O_7$ precipitates from this melt. The lack of YDS in the bottom 10–20 µm of the Al_2O_3 scale is attributed to the low oxygen activity, as mentioned above. The mechanism of transport of Y within the $Mo_5(Si,Al)_3$ layer has not been studied in this work. However, it is considered likely that Y is transported in the form of Y^{3+}, along Al_2O_3 grain boundaries present in this layer and along $Mo_5(Si,Al)_3$/pore interfaces. Previously, it has been reported that Y^{3+} segregates to and is transported along grain boundaries in the oxide scales formed on Y-containing Al_2O_3-forming alloys, both when Y was added to the substrate as oxide particles and in elemental form [27–30].

Yttrium Increases the Oxidation Rate, Scale Spallation and Mass Loss

It is argued that the presence of YDS in the oxide scale contributes to the faster oxide growth of the Y-containing materials. As noted above, the dendritic morphology of YDS, which was observed both at the oxide/gas interface, (Fig. 6) and within the oxide scale (Fig. 7), indicates that the phase has precipitated from a melt. It may be noted that while no melts appear along the SiO_2–Al_2O_3 binary at 1500 °C [31, 32], a melt does occur in the SiO_2–Al_2O_3–Y_2O_3 system at the same temperature, being in equilibrium with mullite and $Y_2Si_2O_7$, see phase diagrams reported by Mao et al. [32]. The eutectic temperature in the SiO_2–Al_2O_3–Y_2O_3 system is reported to be well below 1400 °C [33, 34]. The ability of the SiO_2–Al_2O_3–Y_2O_3 system to form a liquid at the experimental temperature and the dendritic morphology of YDS thus allow us to conclude that a melt has been present in the outer part of the scale. The exact composition of the melt cannot be determined unless samples are quenched from high temperature. The presence of a melt goes a long way towards explaining the increased scale growth, because the liquid phase speeds up the transport of reactants, effectively short-circuiting part of the protective Al_2O_3 scale. In contrast, the protectiveness of the bottom part of the oxide scale is not expected to be affected by melts because it does not contain YDS or mullite.

While the gravimetric measurements of scale spallation are not quantitative, they still indicate that scale spallation increases with the Y-content of the material (Fig. 2b). We note that the scale/substrate interface in the Y added materials is the same as in the reference material (i.e. between Al_2O_3 and $Mo_5(Si,Al)_3$), and that amount of mullite and YDS in the scale is relatively low. It is therefore not expected

to affect the average CTE of the scale significantly and thereby promote spallation. This is consistent with the observation that no increase in the density of cracks or porosity near the oxide/substrate interface has been observed with increasing Y content. Instead, we suggest that the spallation occurs along grain or phase boundaries within the oxide itself, as stresses are built up during cooling due to differences in Young's modulus, coefficient of thermal expansion (CTE) and Poisson's ratio between the phases. For example, the CTE of Al_2O_3 (9.0×10^{-6} K^{-1} [35] is almost a factor of two higher than that of mullite (5.45×10^{-6} K^{-1} [36]) below 1000 °C, which could induce local stresses high enough for spallation. It is also possible that the multi-phase oxide is more prone to spall due the presence of relatively weak and complex phase boundaries (for example mullite/YDS).

Conclusions

The results from this study are summarised in the following points:

- The ability of a $Mo(Si,Al)_2$ composite to resist oxidation in air at 1500 °C is impaired by the addition of 0.1–2.0 wt% Y, the doped materials suffering more scale spallation and faster oxidation.
- The faster oxidation kinetics and high spallation of the Y-containing materials is attributed to the appearance of liquid phase in the oxide scale and to the multiphase nature of the scale which results in thermal stresses which cause spallation.
- The preferential oxidation of Al in $Mo(Si,Al)_2$ is less pronounced in the presence of Y, resulting in a higher concentration of Si(IV) in the scale compared to the undoped material.
- Y, which was added in elemental form, reacts to form $Y_3Al_5O_{12}$ (YAG) during the processing of the composite. During oxidation, the YAG phase dissolves in the $Mo_5(Si,Al)_3$ layer present underneath the oxide scale. Upon entering the outer part of the oxide scale, Y^{3+}, forms a melt belonging to the (Y, Si, Al, O) system. Upon cooling, yttrium disilicate and mullite precipitate from the melt.

Declarations

Conflict of interest Aina Edgren and Erik Ström are employees of Kanthal AB, a manufacturer of commercial heating elements.

References

1. S. Madeddu, F. Ueckerdt, M. Pehl, et al., *Environmental Research Letters* **15**, 2020 124004.
2. United States Department of Energy Office of Energy Efficiency and Renewable Energy, Industrial Technologies Program. *Improving Process Heating System Performance—A Sourcebook for Industry*, 2nd edn. (Industrial Technologies Program, 2007).
3. L. Ingemarsson, K. Hellström, S. Canovic, et al., *Journal of Materials Science* **48**, 2013 (1511).
4. L. Ingemarsson, K. Hellström, L. G. Johansson, J. E. Svensson, and M. Halvarsson, *Intermetallics.* **19**, 2011 (1319).
5. M. Halvarsson, T. Jonsson, L. Ingemarsson, M. Sundberg, J. E. Svensson, and L. G. Johansson, *Materials at High Temperatures* **26**, 2009 (137).
6. M. Sundberg, G. Malmqvist, A. Magnusson, and T. El-Raghy, *Ceramics International.* **30**, 2004 (1899).
7. D. A. Berztiss, R. R. Cerchiara, E. A. Gulbransen, F. S. Pettit, and G. H. Meier, *Materials Science and Engineering A.* **155**, 1992 (165).
8. T. C. Chou and T. G. Nieh, *Journal of Materials Research* **8**, 1993 (214).
9. S. Melsheimer, M. Fietzek, V. Kolarik, A. Rahmel, and M. Schütze, *Oxidation of Metals* **47**, 1997 (139).
10. C. E. Ramberg and W. L. Worrell, *Journal of the American Ceramic Society* **85**, 2002 (444).
11. A. A. Sharif, *Journal of Materials Science* **45**, 2010 (865).
12. F. Liu, H. Götlind, J. E. Svensson, L. G. Johansson, and M. Halvarsson, *Oxidation of Metals* **74**, 2010 (11).
13. P. Y. Hou, *Oxidation of Metals* **52**, 1999 (337).
14. A. Strawbridge and P. Y. Hou, *Materials at High Temperatures* **12**, 1994 (177).
15. L. Yu, Y. Zhang, T. Fu, J. Wang, K. Cui, and F. Shen, *Coatings.* **11**, 2021 (1144).
16. K. Yanagihara, T. Maruyama, and K. Nagata, *Intermetallics.* **4**, 1996 (S133–S139).
17. S. Majumdar, B. Dönges, B. Gorr, H. J. Christ, D. Schliephake, and M. Heilmaier, *Corrosion Science* **90**, 2015 (76).
18. B. Gorr, L. Wang, S. Burk, et al., *Intermetallics.* **48**, 2014 (34).
19. S. Majumdar, D. Schliephake, B. Gorr, H. J. Christ, and M. Heilmaier, *Metallurgical and Materials Transactions A: Physical Metallurgy and Materials Science* **44**, 2013 (2243).
20. K. Yanagihara, T. Maruyama, and K. Nagata, *Intermetallics.* **3**, 1995 (243).
21. S. Lohfeld, M. Schütze, A. Böhm, V. Güther, R. Rix, and R. Scholl, *Materials and Corrosion* **56**, 2005 (149).
22. L. Ingemarsson, M. Halvarsson, J. Engkvist, et al., *Intermetallics* 2010. https://doi.org/10.1016/j.intermet.2009.10.019.
23. A. Edgren, E. Ström, R. Qiu, L. Frisk, F. Akhtar, and Colliander M. Hörnqvist, *Materials Science and Engineering A.* **849**, 2022 143387.

24. I. Barin and G. Platzki, *Thermochemical Data of Pure Substances*, (WCH, Weinheim, 1995).
25. K. Yanagihara, K. Przybylski, and T. Maruyama, *Oxidation of Metals* **47**, 1997 (277).
26. T. Tabaru, K. Shobu, H. Hirai, and S. Hanada, *Intermetallics.* **11**, 2003 (721).
27. B. A. Pint, *Oxidation of Metals* **45**, 1996 (1).
28. K. Yanagihara, K. Przybylski, and T. Maruyama, *Oxidation of Metals.* **47**, 1997 (277).
29. G. J. Tatlock, D. Ram, and P. Wang, *Materials at High Temperatures* **26**, 2014 (293). https://doi.org/10.3184/096034009X463899.
30. D. L. Ram, G. J. Tatlock, and U. Falke, *Materials at High Temperatures.* **22**, 2014 (497). https://doi.org/10.1179/mht.2005.060.
31. H. Mao, M. Selleby, and B. Sundman, *Journal of the American Ceramic Society* **88**, 2005 (2544).
32. H. Mao, M. Selleby, and O. Fabrichnaya, *Calphad. Computer Coupling of Phase Diagrams and Thermochemistry* **32**, 2008 (399).
33. U. Kolitsch, H. J. Seifert, T. Ludwig, and F. Aldinger, *Journal of Materials Research* **14**, (2), 1999 (447).
34. R. K. Ball, M. H. Lewis, A. Szweda, and E. Butler, *Materials Science and Engineering* **71**, 1985 (145).
35. T. Tabaru, K. Shobu, M. Sakamoto, and S. Hanada, *Intermetallics.* **12**, 2004 (33).
36. G. Brunauer, F. Frey, H. Boysen, and H. Schneider, *Journal of the European Ceramic Society* **21**, 2001 (2563).